Surface-plasmon enhancement of Brillouin light scattering from gold-nanodisk arrays on glass†

Z. N. Utegulov*[a, b], J. M. Shaw [c], B. T. Draine [d], S. A. Kim [a] and W. L. Johnson [a]

[a] Materials Reliability Division, National Institute of Standards and Technology, 325 Broadway, Boulder, CO, USA 80305
[b] Department of Physics, University of Cincinnati, Cincinnati, OH, USA 45221
[c] Electromagnetics Division, National Institute of Standards and Technology, 325 Broadway, Boulder, CO, USA 80305
[d] Department of Astrophysical Sciences, Princeton University, Princeton, NJ, USA 08544

ABSTRACT

Enhancement of Brillouin light scattering (BLS) at the wavelength of 532 nm was observed from Rayleigh-like and Sezawa-like acoustic modes of alkaline-earth boro-aluminosilicate glass covered with periodic arrays of gold nanodisks. This enhancement is attributed to mediation of surface plasmons of the nanodisks. For nanodisks with diameters of 71 nm to 90 nm, heights of 30 nm, and periodicity of 100 nm, the maximum measured surface-plasmon enhancement of BLS intensity was, respectively, ~ 2.4 and ~ 5.6 for Rayleigh-like and Sezawa-like modes, relative to the intensity from a gold film with the same fractional coverage area but without surface-plasmon coupling. The maximum for the Rayleigh-like modes occurs with the smallest-diameter nanodisks, and that for the Sezawa-like modes occurs with the largest-diameter nanodisks. The angular dependence is relatively broad. Calculations employing the discrete dipole approximation were used to predict the electric-field intensities in the gold disks and nearby glass as a function of nanodisk diameter. The average calculated intensity at the top surface of the gold increases with decreasing diameter, consistent with the experimental results for Rayleigh-like modes and the expectation that surface ripple is the dominant scattering mechanism for such modes. The results of this study suggest that nanodisk arrays can provide a platform for practical implementation of surface-enhanced BLS analogous to other surface-enhanced spectroscopies, and suggest the additional possibility of substantially extending the range of wave numbers in BLS through plasmonic-crystal band folding.

Keywords: Acoustic waves, Brillouin light scattering, Brillouin scattering, enhancement, gold, nanodisks, array, phonons, surface plasmons, thin films

1. INTRODUCTION

Enhancement of electromagnetic fields through resonant coupling to surface plasmons has been employed to increase signals in a number of optical spectroscopies, including Raman [1, 2], Rayleigh [3, 4], fluorescence [5, 6], and absorption [7, 8]. However, surface-plasmon enhancement of Brillouin light scattering (BLS) has been achieved only with Ag thin films on glass over very narrow ranges of incident angles [9-15]. The potential advantages of implementing more generally applicable surface enhanced BLS (SEBS) spectroscopy are substantial. BLS has been used to measure the elastic and magnetic properties of a wide variety of bulk and thin-film materials through scattering from thermally excited acoustic waves and spin waves, and it is an especially powerful nondestructive technique for characterizing nanoscale thin films and structures, because of the relatively short acoustic or spin wavelengths (hundreds of nanometers) that are involved. However, particularly with respect to nanoscale materials, relatively low signal-to-noise ratios and associated long acquisition times can be a serious impediment to the practical application of BLS.

* email: utegulov@boulder.nist.gov; phone: +1-303-497-4872; fax: +1-303-497-5030;

Plasmonics: Metallic Nanostructures and Their Optical Properties V, edited by Mark I. Stockman,
Proc. of SPIE Vol. 6641, 66411M, (2007) · 0277-786X/07/$18 · doi: 10.1117/12.735253

Surface-plasmon coupling in BLS was originally proposed by Fukui and co-workers [16, 17] for a noble-metal film in an attenuated-total-reflection (ATR) geometry. In this case, light passes through a glass prism to the metal film at the critical angle of maximum transfer of light into the film, optical fields resonantly excite surface plasmons in the film, and surface plasmons inelastically scatter from acoustic surface waves at the metal-air interface. The dispersion curves of light in air and surface plasmons at the continuous air/metal interface do not overlap (so that surface plasmons cannot be excited by light incident on this interface), but this is not a problem at the glass/metal interface, where the optical wavelengths are shorter. Since the theoretical work of Fukui and coworkers, there have been several experimental studies of SEBS from thin flat [9, 10, 12, 13, 15] and periodically corrugated [11, 14] Ag films. For both of these types of geometry, the largest BLS signals were achieved over a very narrow range of incident angles for which the internal (glass/metal interface) reflectivity was a minimum. Due to continuity of the solid Ag films, the surface plasmons involved were of extended nature, rather than localized.

In this paper, we present results of surface-plasmon enhancement of BLS peaks from acoustic modes of arrays of Au nanodisks on a glass substrate. This work is envisioned as the first step towards implementing SEBS metrology on arbitrary samples through the use of noble-metal nanodisk arrays that are brought within a few nanometers of the sample. The potential advantages of noble-metal nanodisk arrays relative to blanket noble-metal films are:

1) the degree of coupling to surface plasmons can be tuned by array geometry and substrate composition,
2) a broader range of incident angles is feasible,
3) the Brillouin scattering of surface plasmons will involve some degree of coupling to acoustic waves or spin waves with shorter wavelengths and corresponding sensitivity to variations in elastic or magnetic properties of samples over smaller scales than is achievable with conventional BLS.

The last of these arises from the fact that surface-plasmon excitation in the nanodisks will introduce electromagnetic field enhancements over nanometer scale distances, and this will lead to inelastic coupling to acoustic or spin modes with correspondingly high wave numbers, Because of the two-dimensional periodicity of the nanodisk array, this effect corresponds to plasmonic-crystal band folding within the lattice formed by the nanodisks, so that momentum conservation in the inelastic scattering of surface plasmons from acoustic or spin waves can involve the addition of a reciprocal lattice vector of the array.

In the following section, the fabrication of the nanodisk arrays is described. In Section 3, the BLS measurement technique is described, and spectra are presented for a blanket Au film on a glass substrate, bare glass, and one of the Au nanodisk arrays as a function of incident angle. Based on the relative frequencies and the polarization dependence of the spectra, two of the peaks from the array are identified as being similar to Rayleigh-like[±] and Sezawa surface acoustic modes of the Au film on glass. The nature of two additional modes of the nanodisk sample also is briefly discussed. Experimental results on surface-plasmon-mediated enhancement of the Rayleigh-like and Sezawa-like[§] modes of Au nanodisk arrays are presented as a function of nanodisk diameter and incident angle of the light. Finally, in Section 4, results of numerical modeling are presented for the electric field distributions in the Au nanodisks and glass as a function of diameter, and the trends of the diameter dependence are compared with the experimental results to provide insight into the principal regions of the material where the BLS enhancement occurs.

2. SPECIMEN FABRICATION

The Au nanodisk arrays were prepared by electron-beam lithography (EBL) on 1.1 mm thick Corning Eagle 2000 alkaline earth boroaluminosilicate glass substrates[#]. First, glass substrates were ultrasonically cleaned in consecutive baths of high purity acetone and isopropanol. The substrates were then immediately loaded into an evaporation chamber and exposed to an Ar plasma for 30 s to further rid the surface of contaminants. A gold layer of 30 nm thickness was then evaporated onto the glass substrate at a rate of ~ 0.6 nm / s. The thickness was monitored with a quartz crystal

[±] True Rayleigh modes occur only at the surfaces of homogeneous bulk materials. In blanket or patterned films (e.g., nanodisk arrays) on a substrate, acoustic modes similar to Rayleigh modes will exist, and these are referred to here as "Rayleigh-like"

[§] True Sezawa modes occur only in thin films on substrates. In substrate-supported nanodisk arrays, acoustic modes similar to the Sezawa modes will exist, and these are referred to here as "Sezawa-like"

[#] The identification, in this document, of this commercially manufactured material does not imply recommendation or endorsement by the National institute of Standards and Technology; nor does it imply that this product is necessarily the best available for the purpose.

monitor (QCM). The QCM was calibrated with a profilometer and thickness standard. The uncertainty in thickness was less than 10 %. An etch mask consisting of cross-linked polymethyl methacrylate (PMMA) was formed on the surface using EBL and was subsequently developed in acetone. A 300 eV Ar^+ mill was used to transfer the etch mask pattern to the Au layer. This process was carefully calibrated to ensure that all the unmasked Au was removed and no significant milling of the substrate occurred. Following the ion mill, the sample was exposed to an oxygen plasma to remove the remaining PMMA masking material.

The etch mask was designed to simultaneously provide nine arrays of 30 nm thick Au nanodisks with a periodicity Δ of 100 nm and diameters D ranging from 70.5 to 90.3 nm. Each array extended over a 40 μm × 40 μm square area on the glass substrate. Figure 1 shows an image of a section of a nanodisk array with D = 70.5 nm, obtained with a field-emission scanning electron microscope (FESEM). To provide a reference in measurements of BLS scattering intensity, a uniform Au film was included in the etch mask, in addition to the array patterns. This film also extended over a 40 μm × 40 μm square area.

3. EXPERIMENTAL RESULTS

The experimental system employed a solid-state diode-pumped frequency-doubled Nd:Vanadate (ND:YVO_4) laser, operating in a single transverse electromagnetic (TEM_{00}) mode, which provided linearly polarized 532 nm light that was focused onto the sample. The profile of the beam at the focus was approximately Gaussian with a diameter of 21 μm. The measurements were performed in a conventional backscattering configuration, with the inelastically scattered light collected through the same lens that was employed to focus the incident laser beam (180º backscatter) and with the normal of the sample surface tilted at various angles θ relative to the axis of the incident beam to vary the component of the photon wave vector parallel to the surface. The polarization of the incident light was in the scattering plane defined by the surface normal and the axis of the laser beam (p-polarized). The 25 mW laser beam was incident from air on the Au-array side of the array/glass sample. The frequency-shifted spectral components of the inelastically backscattered light were analyzed at room temperature with a piezoelectrically scanned (3+3)-pass tandem Fabry-Perot interferometer. The backscattered light was not filtered by a polarizer before passing into the interferometer, except for one case (indicated below) in which a filter was inserted to pass only light polarized perpendicularly to the incident light (cross polarized detection). Light transmitted through the interferometer was detected by a photomultiplier, and the counts were accumulated in a multichannel analyzer during repeated scanning of the interferometer.

Figure 1 defines the coordinate system for the nanodisk arrays in relation to the incident and scattered light. The *z* axis of the sample is defined to be the sample's surface normal, and the light is incident in the *xz* plane from the left in the figure, with a wave-vector component $k_{\|}$ along the *x* axis.

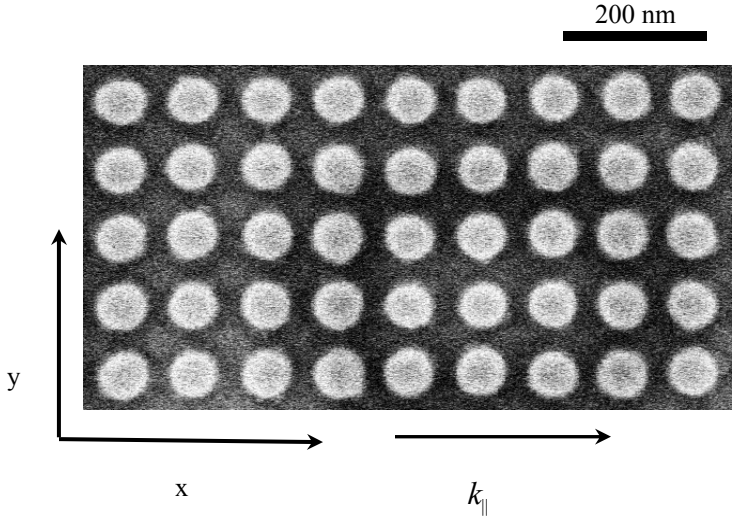

Fig.1. FESEM image of a section of a gold nanodisk array on glass fabricated by EBL. Au disk diameter D = 70.5 nm, array periodicity Δ = 100 nm. The sample *x* and *y* axes are shown, along with the parallel component of the incident photon wave vector $k_{\|}$. The laser beam is incident from air on the Au-disk-array side of the sample.

In Figs. 2(a)-(c) surface BLS anti-Stokes spectra taken at 60º incident angle are shown for the Au blanket film on glass, a bare glass substrate with the same composition, and a nanodisk array on glass with disk diameters D = 86.3 nm. Large peaks centered at a frequency shift of zero in the measured spectra (arising from elastically scattered light) are fit to Gaussian functions and subtracted from the spectra to provide greater clarity in the plots. No polarization filtering was employed in acquiring the spectra of Figs. 2(a)-(c). Figure 2(d) shows a spectrum from the same nanodisk array as 2(c) but with a polarizer inserted in the backscattered light path, such that only light polarized perpendicularly to the incident beam is passed to the interferometer (conventionally denoted as VH detection).

To enable effective discussion of Fig. 2, we note that BLS cross sections from surface acoustic modes of a metallic film are known to be dominated by scattering from the normal components of acoustic displacements (ripple) at the surface of the film [18, 19]. In transparent material without an opaque film on the surface, scattering from bulk acoustic modes can occur from elasto-optic perturbations to the index of refraction.

The two peaks of Fig. 2(a) for the Au film on glass are the well known Rayleigh-like and Sezawa modes (labeled in the figure as R_F and S_F, respectively), which appear as the lowest-frequency peaks in BLS spectra from any uniform opaque metallic film. This spectrum is consistent with earlier BLS measurements from supported gold layers [20]. The lowest-frequency peak R_G in the bare-glass-substrate spectrum (Fig. 2(b)) is the true Rayleigh mode of the half space, which appears at a frequency higher than the R_F peak in the gold because of the higher acoustic velocities of glass. The height of peak R_G is two orders of magnitude smaller than that of R_F, since the lower reflectivity of the glass surface leads to a lower cross section for BLS from the surface ripple. Sezawa modes do not occur in the glass without a film. The higher-frequency peak TA_G in Fig. 2(b) arises from the bulk transverse acoustic mode of the glass and appears at a frequency close to that expected from the shear modulus of 28.9 GPa provided by the manufacturer.

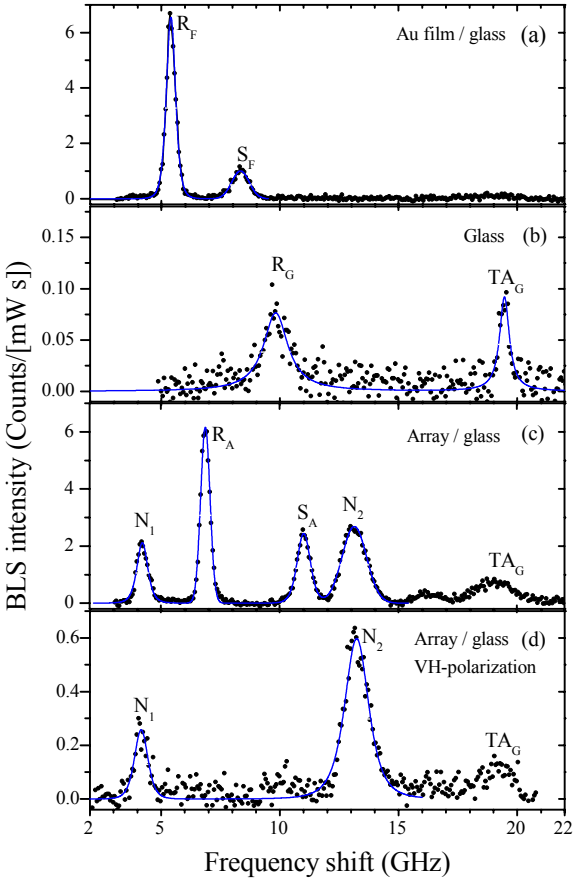

Fig. 2. BLS spectra of (a) Au film on glass, (b) glass, (c) Au nanodisk array on glass with disk diameters D = 86.3 nm, (d) the same Au nanodisk array employing cross-polarized detection.

Additional peaks appear in the spectrum of Fig. 2(c) from the nanodisk array. Since BLS from the Au film serves as a reference for assessing the degree of surface-plasmon enhancement of BLS peaks from the nanodisk arrays, we must determine the correspondence of peaks from the array with peaks R_F and S_F of the Au film. Although the patterning of the Au in the array affects the vibrational displacement patterns of the modes, some of these patterns are expected to remain similar to those in the blanket Au film, as occurs with vibrational modes of nanolines on substrates [21, 22]. Peak R_A in Fig. 2(c) can be assumed to correspond to the Rayleigh-like peak R_F of the film, because it is the strongest and its frequency lies between R_F and R_G, as expected for partial surface coverage of the gold. The frequency of peak R_A (6.9 GHz) is 25 % higher than that of peak R_F (5.5 GHz). A similar fractional shift of the Sezawa mode of the Au film would place the frequency of the corresponding Sezawa-like mode of the array near 10.5 GHz, which is consistent with the observed 11.1 GHz S_A peak in the array (Fig. 2(c)) arising from this mode. Additional evidence for these identifications is provided by the spectrum in Fig. 2(d), which was obtained using a cross-polarization filter inserted in the backscattered light path. Peaks R_F and S_F do not appear in this cross-polarized spectrum, as one would expect from the predominantly surface-ripple scattering that occurs

from Rayleigh-like and Sezawa modes.

The appearance of additional modes (peaks N_1 and N_2) in the nanodisk specimen is interesting, although not directly relevant to the subject of surface-plasmon enhancement considered here. It should be noted that peak N_1 is qualitatively similar to a mode observed in BLS scattering from nanolines [21], in the sense that it is lower in frequency than the Rayleigh-like mode and it appears in VH spectra. This mode in nanolines has been identified as flexural, with shear displacements mainly perpendicular to the scattering plane defined by the incident beam and the surface normal. Higher-frequency flexural modes also appear in BLS from nanolines, and peak N_2 may be analogous to one of these. Weaker BLS peaks above the 22 GHz of Fig. 2 also are observed in the samples, but these are not considered here.

Fig. 3(a) shows measurements of the dispersion curves of the peaks observed in BLS from the Au film on glass and the array on glass with nanodisk diameters D = 86.3 nm. One measurement of the frequency of peak R_G of the bare glass substrate is also included. The range of phonon wave numbers in this figure extends from 18 to 23 μm^{-1}, corresponding to the incident angles ranging from 50º to 75º.

In the remainder of this paper, only the enhancement of the Rayleigh-like and Sezawa-like peaks of the arrays are considered, because the other peaks from the arrays have no corresponding modes in the Au film for comparison. With light incident on a blanket Au film at the Au/air interface, no surface-plasmon excitation occurs, because the dispersion curves of light and surface plasmons do not overlap. However, the Au film does not provide a direct reference for the relative enhancement of BLS scattering from the nanodisk arrays, because the coverage area of the Au is different for the film and an array. Since BLS cross sections from acoustic modes of a metallic film are dominated by ripple scattering, the inelastically scattered intensity is proportional to the area of the film (assuming uniform intensity of incident light). Therefore, the count rate I_{film} of a BLS peak from the blanket Au film must be multiplied by the fractional coverage area γ of a nanodisk array, if it is to be compared with the count rate I_{array} of a corresponding peak from the array, and a measure of the relative BLS enhancement Γ is provided by the following expression:

$$\Gamma = \frac{I_{array}}{I_{film} \times \gamma} = \frac{I_{array}}{I_{film}} \times \frac{\Delta^2}{\left(\pi D^2 / 4\right)} \qquad (1)$$

where I_{array} is the measured BLS count rate from the array at the specified spectral peak, I_{film} is the measured BLS count rate for the peak from the corresponding mode in the Au film, D is the diameter of the nanodisks, and Δ (= 100 nm) is the center-to-center spacing of the nanodisks.

Fig. 3(b) shows values of Γ as a function of wave number for the BLS peaks from the Rayleigh-like (R_A) and Sezawa-like (S_A) modes of the array with D = 86.3 nm. There is enhancement of both the R_A and S_A peaks over the entire measured range of wave numbers (incident angles) with maximum enhancement Γ=5.6 occurring for the Sezawa-like mode at an incident angle of 65º. The maximum Γ for the Rayleigh-like mode is 2.4 at an angle of 55º. Note that Γ is greater than 1 over the entire range of incident angles in Fig. 3, in contrast to ATR-based SEBS approaches mentioned above, which are effective over only a very narrow angular range.

Fig. 4 shows the measured enhancement factors Γ for the R_A and S_A modes as a function of nanodisk diameter at an angle of 60º. The maximum enhancement for the Rayleigh-like mode occurs for the smallest nanodisk size, but varies by just ~10 % over the 20 nm range of diameters. The opposite trend is measured for Sezawa-like mode enhancement, the greatest values of Γ occurring with the largest nanodisks. The changes in Sezawa-like mode enhancement are also much greater over the measured range of diameters.

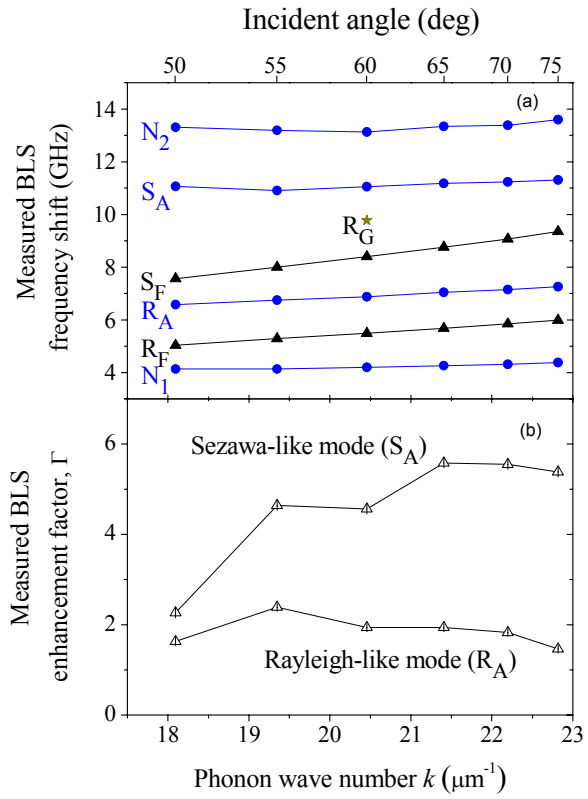

Fig. 3. Phonon-wave-number dependence of (a) BLS frequency shifts for modes in glass, Au film on glass and Au disk array on glass with D = 86.3 nm; (b) BLS enhancement factors Γ for R_A amd S_A modes

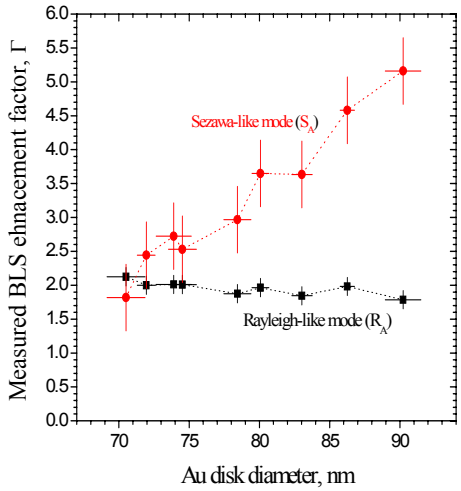

Fig. 4. BLS enhancement factors Γ for Rayleigh-like and Sezawa-like modes of Au nanodisk arrays on glass.

4. NUMERICAL MODELING

Currently, theoretical models have been developed for surface-enhanced BLS cross sections in the ATR configuration for silver film on glass [16-18, 23, 24] and for periodically corrugated silver gratings [25, 26]. However, no model is currently available for BLS cross sections of nanodisk arrays mediated by surface plasmons. Here, we seek qualitative explanations for the measured dependence of Γ on nanodisk diameters by using numerical calculations of surface-plasmon-enhanced electric-field intensity distributions in the arrays.

In considering the Rayleigh-like and Sezawa-like modes in the arrays, we assume that the BLS scattering is dominated by the ripple mechanism at the surfaces of the gold disks. As mentioned above, the dominance of ripple scattering in the BLS cross section in the absence of surface-plasmon enhancement is well established for surfaces of metals. Ripple scattering also has been previously assumed to be dominant mechanism in surface-plasmon enhanced BLS for silver films and gratings on glass in the ATR configuration [17, 23, 24, 26].

4.1. Discrete Dipole Approximation

We have used the discrete dipole approximation (DDA) [27-29] to calculate the electromagnetic field within targets with the geometry of the Au nanodisk arrays studied here with BLS. Each target consists of a uniform glass slab with an infinite array of Au nanodisks located on one surface. The target is illuminated by a linearly polarized plane wave incident at an angle θ relative to the surface normal. The calculations were carried out using a new version of the DDSCAT code [30]. The targets were represented by dipole arrays, with an interdipole spacing of 5 nm.

The target's unit cell in the DDA calculations consisted of a gold nanodisk with a height of 30 nm on a cube of alkaline-earth boro-aluminosilicate glass that was 100 nm on each edge. The dielectric constant of gold at λ=532nm was taken to be 0.528 +2.23i, based on interpolation of values reported by Johnson and Christy [31] for an evaporated gold film. The refractive index of the glass at the same wavelength is 1.510, based on interpolation of values provided by the manufacturer.

The results of DDA calculations for nanodisk arrays with D = 70.5 nm and 90.2 nm diameters (the smallest and largest nanodisks measured in BLS) are shown in Fig. 5 as two-dimensional color-coded contour plots of electric field intensity $|E|^2$ normalized to the incident light intensity $|E_0|^2$. The incident light is polarized in the *xz* plane, the incident angle of the light is 60º, and the parallel component of the incident photon wave vector $k_{||}$ lies along the positive *x*-direction. Figures 5(a) and 5(b) show the normalized intensities at the top surface (the gold/air interface) of the 70.5 nm and 90.2 nm nanodisks, respectively, and Figs. 5(c) and 5(d) show the corresponding intensities at the lower (Au/glass) interface. These results illustrate the fact that arrays with smaller disks are found to have higher overall intensities at the top surface, especially near the edges, compared to the intensities in the larger disks at this surface. As shown in Figs. 5(c) and 5(d), the trailing corners at the Au/glass/air interface (away from the incident light) have "hot" spots. No similar high-intensity regions are present at the trailing edges at the top of the nanodisks. This phenomenon can also be seen in the plots of the mid-cross-sectional *xz*-planes (Figs. 5(e) and 5(f)). The maximum calculated values for the intensity occur close to the lower interface (at $z \sim -1$ nm) in both nanodisk arrays of Fig. 5.

Average normalized electric field intensities over the top and bottom surfaces of Au disks are plotted in Fig. 6 as a function of nanodisk diameter, with the selected discrete values of the diameters equal to those of the samples measured with BLS. For both the top and bottom surfaces, the general trend of higher intensities at lower diameters in the calculated curves in Fig. 6 is consistent with the trend of the measured BLS enhancements of Rayleigh-like modes (R_A) of the nanodisk arrays (Fig. 4).

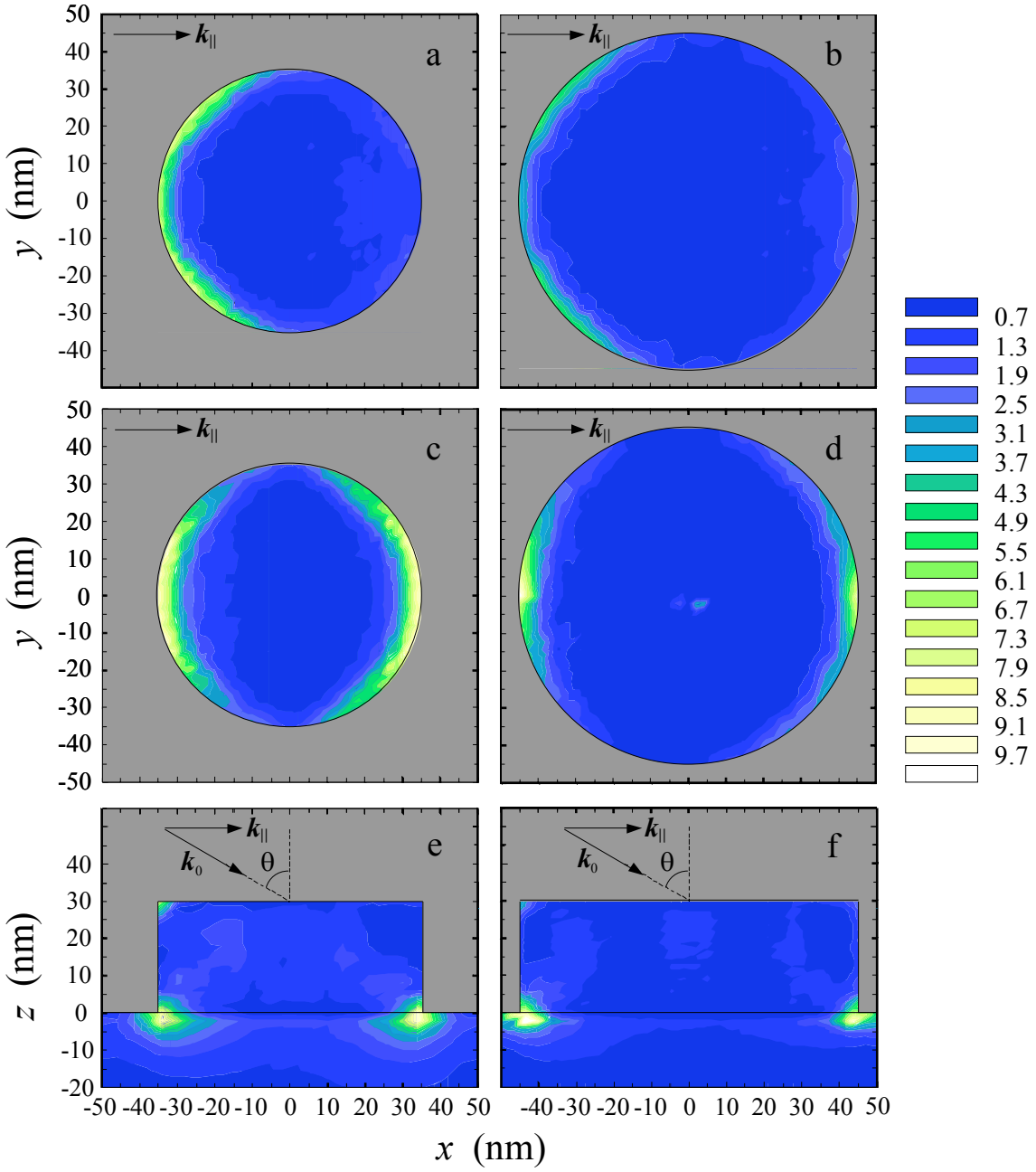

Fig. 5. Distributions of electric-field intensity $|E|^2$ (normalized with respect to the incident light intensity $|E_0|^2$) on the top surface of Au nanodisks with diameters of (a) 70.5 nm and (b) 90.2 nm and on the bottom surface with diameters of (c) 70.5 nm and (d) 90.2 nm. Distributions in the cross-sectional *xz* plane at y = 0 for nanodisks with diameters of (e) 70.5 nm and (f) 90.2 nm diameters. The incident phonon wave vector $\boldsymbol{k}_0$ and surface-parallel component of the wave vector $\boldsymbol{k}_{||}$ are indicated in the figure.

The results of the calculations shown in Fig. 6 do not explain the measured dependence of the Sezawa-like mode on diameter. In considering possible explanations for this dependence, it is useful to note that the displacement patterns of the Rayleigh-like and Sezawa-like modes in nanodisk arrays differ from the corresponding blanket-film modes, even though they are expected to be qualitatively similar, and actual displacements amplitudes are expected to vary significantly over the *xy* planes at both the top and bottom surfaces. In particular, the magnitudes of acoustic stress near the corners of the nanodisks (where the electric fields are greatest) are expected to depend on the diameter, and this will affect the dependence of the enhancement factors on diameter.

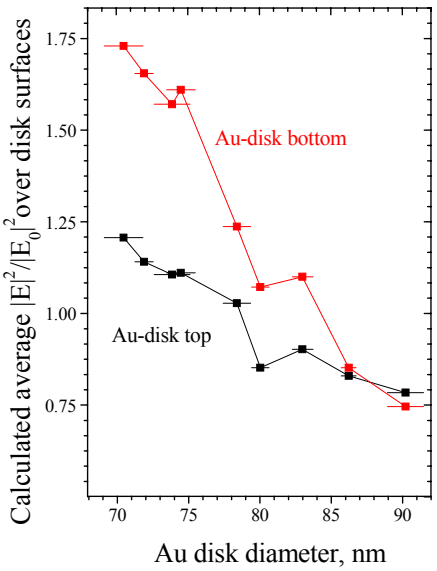

Fig. 6. Calculated average normalized electric-field intensities over the top and bottom disk surfaces versus disk diameter.

5. CONCLUSION

This study has demonstrated surface-plasmon enhancement of BLS from Au nanodisk arrays on a glass substrate with the light incident on the surface of Au nanodisks over a relatively broad range of angles. The results suggest the possibility of developing practical methods for enhancement of BLS intensities from acoustic waves and spin waves in a wide variety of material systems using nanodisk arrays that are placed in nanometer-scale proximity to the surfaces of samples. Perhaps even more intriguing is the possibility of extending BLS measurements to wave numbers much greater than that of the incident light through the introduction of significant nanometer-scale variations in the electric field (as in Fig. 5), corresponding to the addition of reciprocal lattice vectors of the array through plasmonic-crystal band folding. With array periodicities on the order of 100 nm, the addition of reciprocal lattice vectors to the scattering acoustic or spin wave numbers would lower the detectable wavelengths into the range of a few tens of nanometers and provide sensitivity to the properties of surface layers with thicknesses approaching those of atomic monolayers.

ACKNOWLEDGEMENT

We thank Roy Geiss for FESEM imaging of the Au nanodisk arrays.

REFERENCES

1. J. A. Dieringer, A. D. McFarland, N. C. Shah, D. A. Stuart, A. V. Witney, C. R. Yonzon, M. A. Young, X. Zhang, R. P. Van Duyne, "Surface enhanced Raman spectroscopy: new materials, concepts, characterization tools, and applications" Faraday Discuss., 132, 3-8 (2006)
2. L. Qin, S. Zou, C. Xue, A. Atkinson, G. C. Schatz, C. A. Mirkin, "Designing, fabricating and imaging Raman hot spots", PNAS, 103(36), 13300-13303 (2006)
3. T. Itoh, V. Biju, M. Ishikawa, Y. Kikkawa, K. Hashimoto, A. Ikehata, Y. Ozaki, "Surface-enhanced resonance Raman scattering and background light emission coupled with plasmon of single Ag nanoaggregates" J. Chem. Phys., 124, 134708 (2006)
4. M. A. Noginov, G. Zhu, M. Bahoura, J. Adegoke, C. Small, B. A. Ritzo, V. P. Drachev, V. M. Shalaev, "The effect of gain and absorption on surface plasmons in metal nanoparticles", Appl. Phys. B 86, 455-460 (2007)
5. P. Bharadwaj, P. Anger, L. Novotny, "Nanoplasmonic enhancement of single-moelcule fluorescence", Nanotechnology 18, 044017 (2007)
6. P. Johansson, H. Xu, M. Kall, "Surface-enhanced Raman scattering and fluorescence near metal nanoparticles", Phys. Rev. B 72, 035427 (2005)
7. M. Gadenne, V. Podolskiy, P. Gadenne, P. Sheng, V. M. Shalaev, "Plasmon-enhanced absorption by optical phonons in metal-dielectric composites", Europhys. Lett. 53(3), 364-370 (2001)
8. M. S. Anderson "Surface enhanced infrared absorption by coupling phonon and plasmon resonance", Appl. Phys.

Lett. 87, 144102 (2005)
9. A. L. Moretti, W. M. Robertson, B. Fisher, R. Bray, "Surface-enhanced Brillouin scattering on silver films", Phys Rev B, 31(6), 3361-3368 (1985)
10. W. M. Robertson, A. L. Moretti, R. Bray, "Surface-plasmon-enhanced Brillouin scattering on silver films: Double-resonant effect", Phys. Rev. B, 35(17), 8919-8928 (1987)
11. W. M. Robertson, M. Grimsditch, A.L. Moretti, R. G. Kaufman, G. R. Hulse, E. Fullerton and I. K. Schuller, "Brillouin scattering from corrugated Ag films: surface-plasmon-mediated enhancement and relaxed wave-vector conservation", Phys. Rev. B, 40, 4153-4156 (1989)
12. S. Lee, B. Hillebrands, J. R. Dutcher, G. I. Stegeman, W. Knoll, F. Nizolli, "Dispersion and localization of guided acoustic modes in a Langmuir-Blodgett film studies by surface-plasmon-polariton-enhanced Brillouin scattering",
Phys. Rev. B 41(8), 5382-5387 (1990)
13. F. G. Gleed, B. Hillebrabds, S. Lee, G. I. Stegeman and J. R. Sambles, "The angular dependence of surface-enhanced Brillouin scattering from silver in double resonance configuration", Sol. St. Comm., 70(3), 237-239 (1989)
14. W. M. Robertson, M. Grimsditch, A. L. Moretti, R. G. Kaufman, G. R. Hulse, E. Fullerton, I. K. Schuller, "Light scattering by surface acoustic waves on corrugated metal surfaces", Phys. Rev. B, 41(8), 4986-4992 (1990)
15. R. Eberle, T. Kresser, M. Pietralla, "Elastic properties of thin silver films: hexagonal model and influence of corrugation effects", Thin Solid Films, 408, 169-175 (2002).
16. M. Fukui, O. Toda, V. C. Y. So, G. I. Stegeman, "Surface plasmon enhanced Brillouin scattering from metal films", Solid State Communications, 36, 995-1000 (1980)
17. M. Fukui, O. Tada, V. C. Y. So, G. I. Stegeman, "Enhanced Brillouin scattering involving surface plasmon polaritons", J Phys. C: Sol. St. Phys, 14, 5591-5607 (1981)
18. L. Bassoli, F. Nizolli, J. R. Sandercock, "Surface Brillouin scattering in polycrystalline gold", Phys. Rev. B, 34(2), 1296-1299 (1986)
19. R. Loudon, "Theory of surface-ripple Brillouin scattering by solids", Phys. Rev. Lett., 40(9), 581-583 (1978)
20. B. Hillebrands, P. Baumgart, R. Mock, G. Guntherodt, "Dispersion of localized elastic modes in thin supported gold layers measured by Brillouin scattering", J. Appl. Phys., 58(8), 3166-3168 (1985)
21. R. D. Hartschuh, A. S. Kisiluk, V. Novikov, P. Sokolov, P. R. Heylinger, C. M. Flannery, W. L. Johnson, C. L. Soles, W.-L. Wu "Acoustic modes and elastic properties of polymeric nanostructures", Appl. Phys. Lett. 87, 173121 (2005)
22. W. L. Johnson, C. M. Flannery, S. A. Kim, R. Geiss, C. L. Soles, P. R. Heyliger, W. Hu, S. W. Pang, "Elastodynamic characterization of imprinted nanolines," *Materials Research Society Symposium Proceedings*, 924, 0924-Z08-31 (2006).
23. A. Marvin, V. Bortolani, F. Nozolli, G. Santoro and V. Celli. "Theory of three-wave mixing of volume EM, surface polaritons and surface acoustic waves", J. Phys. C: Sol. St. Phys., 15, 3273-3280 (1982)
24. N. Marucci, F. Nizolli, "Theory of surface-plasmon-polariton-enhanced Brillouin scattering in a metal-dielectric bilayer", Surf. Sci. 236, 175-186 (1990)
25. A. M. Marvin, F. Nizolli, "Theory of Brillouin scattering on a surface grating: role of surface polaritons", Phys. Rev. B, 45(20), 12160-12163 (1992)
26. A. M. Marvin, F. Nizolli, L. Giovannini, "Theory of Brillouin scattering from corrugated surfaces", Phys. Rev. B, 51(15), 10134-10145 (1995)
27. E. M. Purcell, C. R. Pennypacker, "Scattering and absorption of light by nonspherical dielectric grains", Ap.J., 186, 705-714 (1973)
28. B. T. Draine, J. Goodman, "Beyond Clausius-Mossotti: wave propagation on a polarizable point lattice and the discrete dipole approximation", Ap. J., 405, 685-697 (1993)
29. B.T. Draine, P.J. Flatau, "Discrete dipole approximation for scattering calculations", JOSA A 11, 1491-1499 (1994).
30. B. T. Draine, P.J. Flatau, "The Discrete Dipole Approximation for Periodic Targets", in preparation (2007).
31. P. B. Johnson, R. W. Christy, "Optical Constants of the Noble Metals", Phys. Rev. B, 6, 4370-4379, (1972)